IEEE Access
Multidisciplinary : Rapid Review : Open Access Journal

Received August 20, 2018, accepted September 26, 2018, date of publication October 1, 2018, date of current version October 25, 2018.

*Digital Object Identifier 10.1109/ACCESS.2018.2873392*

# Broadband and High-Gain SIW-Fed Antenna Array for 5G Applications

**XIUPING LI, (Senior Member, IEEE), JUN XIAO, ZIHANG QI, (Student Member, IEEE), AND HUA ZHU, (Member, IEEE)**
School of Electronic Engineering, Beijing University of Posts and Telecommunications, Beijing 100876, China
Beijing Key Laboratory of Work Safety Intelligent Monitoring, Beijing 100876, China

Corresponding author: Xiuping Li (xpli@bupt.edu.cn)

This work was supported in part by the Project 6140518040116DZ02001 through the Equipment Development Department of the Central Military Commission, in part by the Project 61601050 through the National Natural Science Foundation of China (NSFC), and in part by the National Science and Technology Major Project of China under Grant 2017ZX03001028-003.

**ABSTRACT** A broadband and high-gain substrate integrated waveguide (SIW)-fed antenna array is demonstrated for 5G applications. Aperture coupling is adopted as the interconnecting method in the two-layer SIW feeding network. Two pairs of metallic posts act as dipoles and are surrounded by an air-filled cavity. The height of the cavity is designed to be higher than that of the posts to broaden the bandwidth. The measured impedance bandwidth of the proposed 8×8 antenna array is 16.3% from 35.4 to 41.7 GHz for $|S_{11}| \leqslant -10$ dB, and the measured peak gain is 26.7 dBi at 40 GHz. The measured radiation efficiency of the antenna array is 83.2% at 40 GHz. The proposed antenna array which is suitable for 5G applications at 37 and 39 GHz bands shows stable radiation patterns, high gain, and broad bandwidth.

**INDEX TERMS** Magneto-electric (ME) dipole, 5G, substrate integrated waveguide (SIW), broadband, high gain, antenna array.

## I. INTRODUCTION

In July, 2016, the Federal Communications Commission (FCC) adopted rules to identify and open up a new Upper Microwave Flexible Use service in the 28 GHz (27.5-28.35 GHz), 37 GHz (37-38.6 GHz), 39 GHz (38.6-40 GHz) bands and an unlicensed band at 64-71 GHz for Next Generation (5G) wireless communication applications [1]. In these communication systems in millimeter-wave (MMW) bands, high-gain antennas with high efficiency are essential due to the huge propagation loss. High-gain antenna arrays always include large number of radiating elements which requires low-loss feeding networks. Microstrip line is a planar transmission line which has been widely utilized in the feeding networks of microwave antenna arrays because of its advantages of low profile and ease of integration. However, it always suffers from high ohmic and dielectric losses at high frequency especially in the large array designs [2]. Waveguide antennas are usually designed to achieve high gain [3]–[5]. However, the large volume of the metallic waveguide and the high fabrication cost are the main obstacle for mass production.

A planar waveguide transmission line called substrate integrated waveguide (SIW) [6] or laminated waveguide [7] has been widely used in the millimeter-wave antenna array designs due to its merits of low losses, low fabrication costs and easy integration [8]–[28]. Planar antenna arrays with multilayered SIW corporate feeding networks have been increasingly investigated in recent years because of its ability to achieve high gain and broad bandwidth [16], [18]–[28]. However, it is difficult to realize multilayered SIW-fed antenna arrays in printed circuit board (PCB) process because of the use of large number of blind and buried vias. Therefore, most of these antenna arrays are designed and fabricated with low temperature co-fired ceramic (LTCC) process with high costs [23]–[28].

Besides the low-loss feeding network, broadband and high-gain antenna element is important to an antenna array. Patch or slot antennas are always adopted as the radiating element due to their simple and compact structures. However, patch or slot arrays usually suffer from narrow impedance bandwidth or unstable radiation patterns in the bandwidth. Magneto-electric (ME) dipole antenna, proposed by Luk and Wong [29], is a complementary antenna which has advantages of broad bandwidth and stable unidirectional radiation patterns with low cross-polarization and low back radiation. It can be a good candidate for composing wideband and high-gain millimeter-wave antenna arrays. Some MMW planar ME dipole antenna arrays have been reported in [30]–[33] and good performances have been achieved.

In this paper, a broadband ME dipole antenna element which is modified from the antenna element presented in [34] is designed. It is composed of two pairs of metallic posts which form two dipoles located on the opposite sides of the feeding slot etched on the SIW. The dipoles are surrounded by an air-filled metallic cavity for better performance. The height of the cavity is higher than that of the dipoles which broadens the bandwidth of the antenna element. A two-layer feeding network is designed in the $2\times2$ subarray. For proof of concept, an $8\times8$ antenna array with a low-loss SIW feeding network is further designed and measured. The measured results show that the proposed antenna array can be applied for 5G applications to cover 37 GHz (37-38.6 GHz), and 39 GHz (38.6-40 GHz) bands.

The paper is organized as follows. Section II presents the geometry of the antenna element. The designs of $2\times2$ subarray and $8\times8$ array are illustrated in Section III. Section IV gives the measured results of the $8\times8$ array, and the conclusion is given in Section V.

## II. ANTENNA ELEMENT DESIGN

The geometry of the antenna element is shown in Fig. 1. The two pairs of metallic posts along $x$-axis work as two electric dipoles which are surrounded by a cavity. The gap between four posts and the two gaps between posts and cavity wall along $y$-axis work as magnetic dipoles [34]. The radiating element is fed by a transverse slot etched on the SIW feed. All the PCBs used in this paper are Rogers 5880 with a relative dielectric constant of 2.2 and thickness of 1.575 mm. The height of the four posts is $h_p = 0.25\lambda_0$ (2 mm), where $\lambda_0$ is the wavelength at 37.5 GHz in free space.

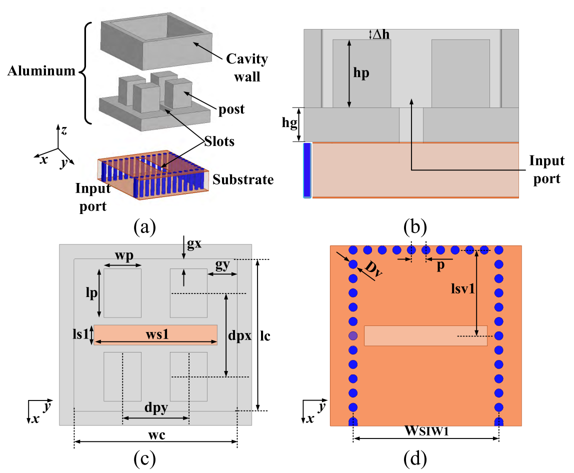


**FIGURE 1.** Geometry of the proposed antenna element. (a) Exploded view. (b) Side view. (c) Top view of the radiating element. (d) Top view of the feeding SIW.

As shown in Fig. 2, the impedance bandwidth for $|S_{11}| \leqslant -10$ dB is 19.6% (35.3-43 GHz) and the peak gain is 8.7 dBi. The simulated radiation patterns in the $E(xoz)$- and the $H(yoz)$-plane at 36, 38, 40, 42 GHz are shown in Fig. 3. It is observed that the proposed antenna element features stable and almost equal unidirectional radiation patterns in two planes. The cross-polarizations are less than −35 dB in two planes. The patterns in both planes are symmetric and the 3-dB beamwidths are all above 60° within the bandwidth. All these characteristics prove that the proposed antenna element is suitable for composing broadband and high-gain large antenna arrays. The optimized dimensions of the proposed antenna element are given in Table 1.

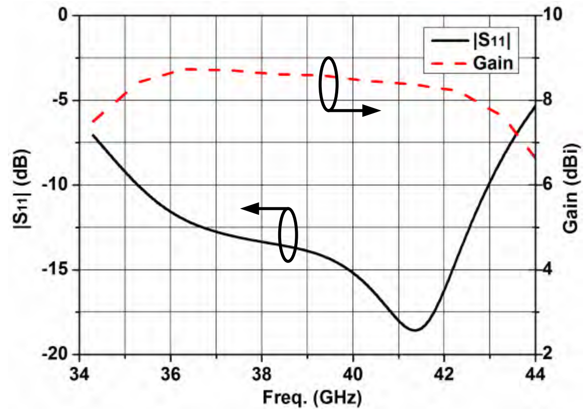


**FIGURE 2.** Simulated $|S_{11}|$ and gain of the proposed antenna element.

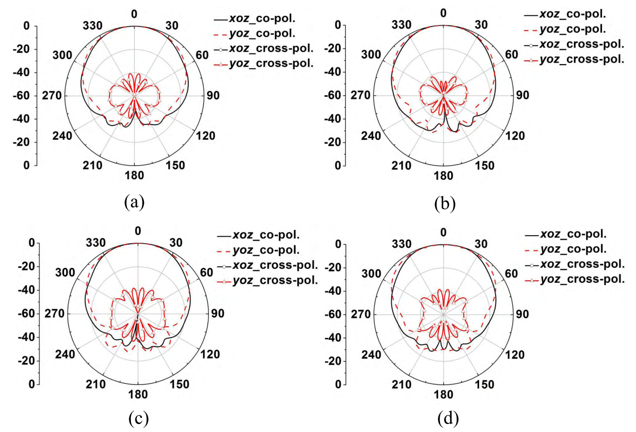


**FIGURE 3.** Simulated radiation patterns of the proposed antenna element at different frequencies. (a) 36 GHz. (b) 38 GHz. (c) 40 GHz. (d) 42 GHz.

**TABLE 1.** Dimensions of The Proposed Antenna Element (Unit:mm).

| | | | | | | | | | |
|---|---|---|---|---|---|---|---|---|---|
| Para. | $h$ | $h_g$ | $\Delta h$ | $h_p$ | $l_p$ | $l_{s1}$ | $w_p$ | $w_{s1}$ | $d_{py}$ |
| Values | 2.3 | 1 | 0.3 | 2 | 1.7 | 0.7 | 1.3 | 4.3 | 2.3 |
| Para. | $w_c$ | $g_x$ | $g_y$ | $d_{px}$ | $l_c$ | $D_y$ | $p$ | $l_{sv1}$ | $W_{SIW1}$ |
| Values | 5.7 | 0.35 | 1.05 | 2.9 | 5.3 | 0.3 | 0.5 | 3.5 | 5.1 |

In this paper, $\Delta h$, the height difference between the posts and the cavity wall, as shown in Fig. 1(b) is introduced to demonstrate the bandwidth enhancement. As shown in Fig. 4 (a), the bandwidth is extended to the lower frequency

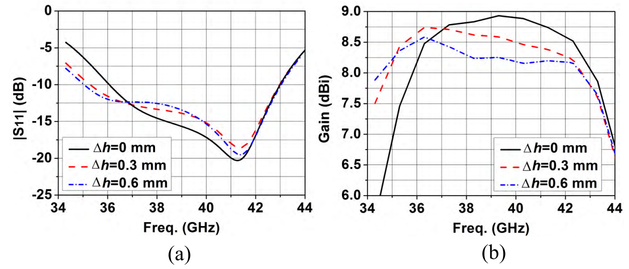


**FIGURE 4.** **Simulated results of the antennas with different $\Delta h$. (a) $|S_{11}|$. (b) Gain.**

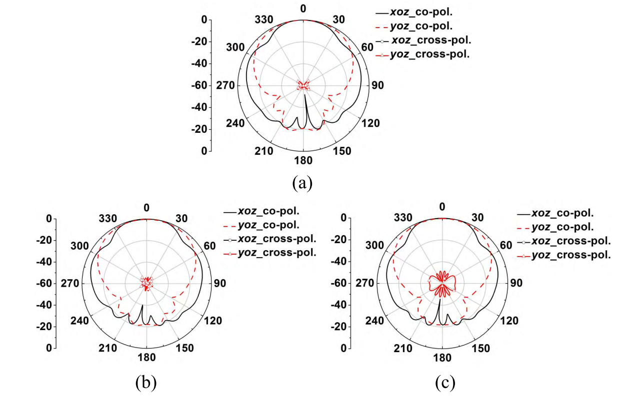


**FIGURE 7.** **Simulated radiation patterns of the referenced antenna without cavity at different frequencies. (a) 38 GHz. (b) 40 GHz. (c) 42 GHz.**

while the higher-end frequency keeps unchanged as $\Delta h$ increases. It is because that the higher cavity ($0 < \Delta h \leq 0.6$ mm) walls further enlarge the effective current path of the electric dipoles which extends the lower frequency band. However, the gain decreases accordingly. To make a trade-off between bandwidth and gain, $\Delta h$ is optimized to be 0.3 mm.

As shown in Fig. 5, a referenced antenna without cavity has been designed to further understand the function of the cavity. In Fig. 6, it can be seen that the cavity improves the impedance bandwidth and enhances the gain in the frequency band from 35 to 42 GHz. The simulated radiation patterns of the referenced antenna without cavity are presented in Fig. 7. Compared with the results in Fig. 3, the uniformity of the radiation patterns in $E$- and $H$-planes deteriorates. The cavity suppresses the back radiation and enhances the boresight radiation. This is because two magnetic dipoles, formed by the two gaps between posts and cavity wall along $y$-axis, have been introduced by adding the cavity structure. The two added magnetic dipoles improve the radiation characteristics of the ME dipole antenna.

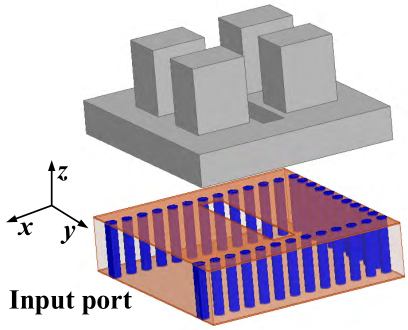


**FIGURE 5.** **Exploded view of the antenna without cavity.**

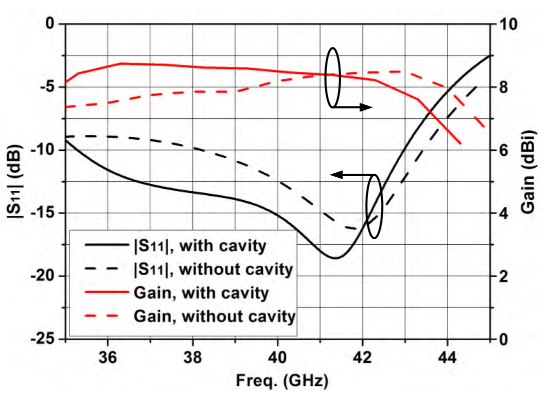


**FIGURE 6.** **Simulated $|S_{11}|$ and gains of the antennas with and without cavity.**

## III. ANTENNA ARRAY DESIGN

### A. 2×2 SUBARRAY

As depicted in Fig. 8, a 2×2 subarray is designed based on the proposed antenna element. The spacings between radiating elements are $d_{ux}=0.725\lambda_0$ (5.8 mm) and $d_{uy}=0.775\lambda_0$(6.2 mm), respectively, where $\lambda_0$ is the wavelength at 37.5 GHz in free space. The two-layer feeding network of the 2×2 subarray is shown in Fig. 9. A slot etched on the SIW in substrate 2 is used to couple the energy from substrate 2 to substrate 1. The coupled energy is divided into four

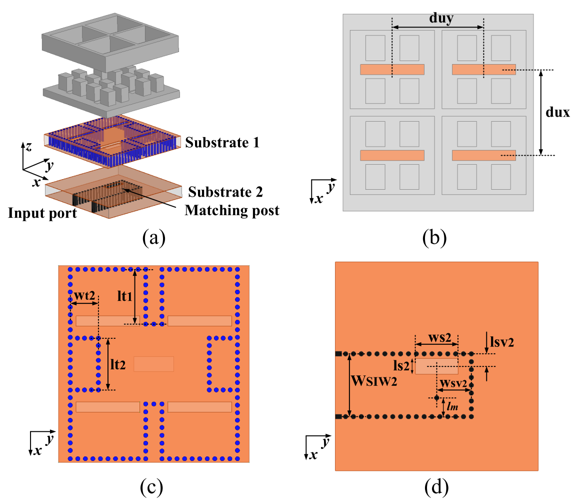


**FIGURE 8.** **Geometry of the proposed 2×2 subarray. (a) 3-D exploded view. (b) Top view of the radiating structures. (c) Top view of the substrate 1. (d) Top view of the substrate 2.**

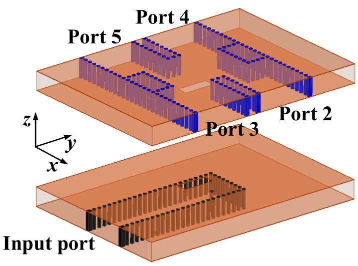


**FIGURE 9.** 3-D exploded view of feeding network of the 2×2 subarray.

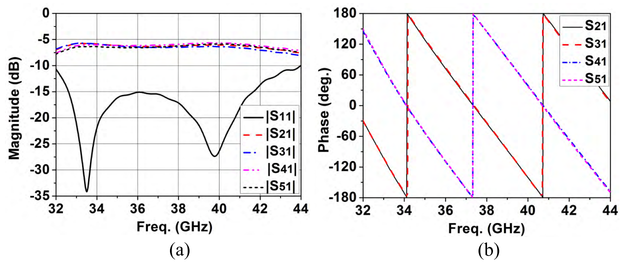


**FIGURE 10.** Simulated results of the two-layer feeding network of 2×2 subarray. (a) S-parameters. (b) Phase.

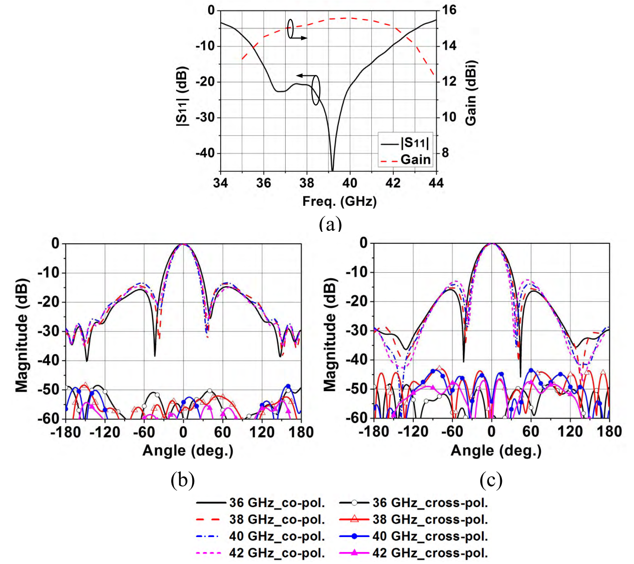


**FIGURE 11.** Simulated results of the proposed 2×2 subarray. (a) $|S_{11}|$ and gains. Simulated radiation patterns at 36, 38, 40, and 42 GHz on (b) *E*-plane (*xoz*-plane) and (c) *H*-plane (*yoz*-plane).

parts to excite the antenna elements. The simulated results of the two-layer four-way power divider is presented in Fig. 10. The power divider has a bandwidth from 31.9 to 44 GHz for $|S_{11}| \leqslant -10$ dB. The outputs at ports 2-5 are almost equal in magnitude within the matching band. It is noted that the outputs at ports at 2 and 3 and the outputs at ports 4 and 5 are out of phase, respectively. The optimized dimensions of the proposed 2×2 subarray are given in Table 2. The simulated results of the 2×2 subarray are given in Fig. 11. The simulated impedance matching bandwidth of the proposed 2×2 subarray for $|S_{11}| \leqslant -10$ dB is 16.6% ranging from 35.5 to 41.9 GHz. The peak gain is 15.6 dBi. The radiation patterns are stable in both planes within the bandwidth. The cross-polarizations are less than −42 dB in two planes.

**TABLE 2.** Dimensions of 2×2 Subarray (Unit:mm).

| Para. | $d_{ux}$ | $d_{uy}$ | $l_{t_1}$ | $w_{t2}$ | $l_{t_2}$ | $l_{s_2}$ | $w_{s_2}$ | $w_{sv_2}$ | $l_{sv_2}$ | $l_m$ | $W_{SIW2}$ |
|---|---|---|---|---|---|---|---|---|---|---|---|
| Values | 5.8 | 6.2 | 3.7 | 1.9 | 3.5 | 1 | 2.7 | 2.2 | 0.8 | 1.2 | 4 |

### *B. 8×8 ARRAY*

For high-gain applications, an 8×8 array antenna with two-layer full-corporate SIW feeding network is designed as shown in Fig. 12. The performances of the H-junctions in substrate 2 have decisive effects on the overall reflection coefficient performance of the 8×8 array. The width of all the SIWs in substrate 2 are set to be 4 mm. Only one type of H-junction is used in the SIW power divider in substrate 2 as shown in Fig. 13. As shown in Fig. 14, the bandwidth of the H-junction is 24.4% ranging from 33.4 to 42.7 GHz for $|S_{11}| \leqslant -20$ dB. The outputs at ports 2-5 are

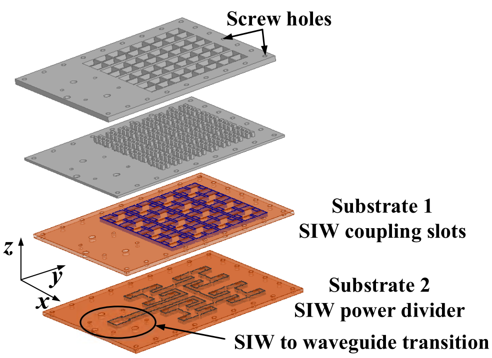


**FIGURE 12.** Configuration of the 8×8 antenna array with two-layer full-corporate SIW feeding network.

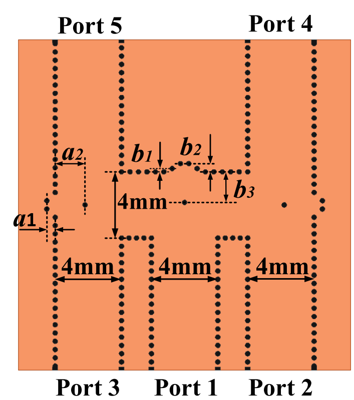


**FIGURE 13.** Configurations of the H-junction used in the SIW power divider in substrate 2.

equal in magnitude and phase. Optimized dimensions of the H-junction are given in Table 3. For the purpose of measurement, a waveguide WR-22 to SIW transition is designed,

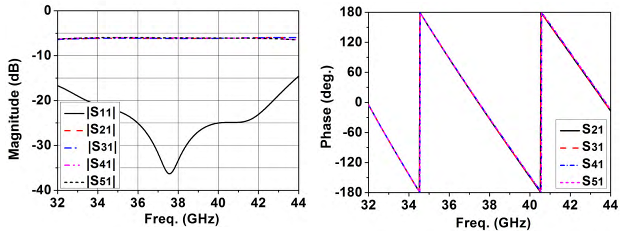


(a) (b)

**FIGURE 14.** Simulated results of the H-junction used in the SIW power divider in substrate 2. (a) S-parameters. (b) Phase.

**TABLE 3.** Dimensions of the H-Junction (Unit:mm).

| Para. | $a_1$ | $a_2$ | $b_1$ | $b_2$ | $b_3$ |
|---|---|---|---|---|---|
| Values | 0.5 | 1.8 | 0.2 | 0.5 | 1.8 |

as shown in Fig. 15. The dimensions of the transition are given in Table 4. The simulated $|S_{11}|$ and $|S_{21}|$ are exhibited in Fig. 16, which shows that the transition has a bandwidth 21.1% from 34.7 to 42.9 GHz for $|S_{11}| \leqslant -15$ dB and an insertion loss less than 0.3 dB within the bandwidth.

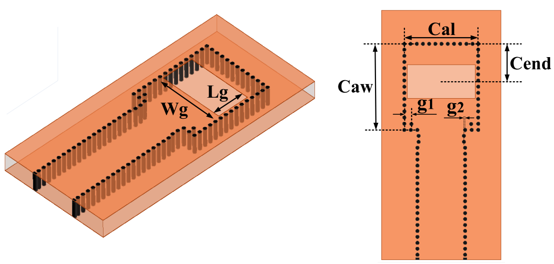


(a) (b)

**FIGURE 15.** Simulated model of the proposed waveguide to SIW transition. (a) 3-D view. (b) Top view.

**TABLE 4.** Dimensions of Waveguide To SIW Transition (Unit:mm).

| Para. | $W_g$ | $L_g$ | $C_{aw}$ | $C_{al}$ | $C_{end}$ | $g_1$ | $g_2$ |
|---|---|---|---|---|---|---|---|
| Values | 5.7 | 2.8 | 7.2 | 6.2 | 3.2 | 0.6 | 0.1 |

## IV. EXPERIMENTS AND DISCUSSIONS

The cavity and posts are fabricated separately by using wire cut electrical discharge machining technology. The feeding network is fabricated using standard single-layer PCB technology as indicated in Fig. 17. The antenna array was measured with the setup shown in Fig. 17(c). The total size of the 8×8 antenna array is 66 mm×85.4 mm×6.6 mm. The simulated and measured $|S_{11}|$ and gains of the fabricated antenna array are shown in Fig. 18. The simulated and measured bandwidths of the antenna array are 16.9% from 35.6 to 42.2 GHz and 16.3% from 35.4 to 41.7 GHz for $|S_{11}| \leqslant -10$ dB, respectively. It fully covers the licensed 5G bandwidth of 37 to 38.6 GHz and 38.6 GHz to 40 GHz. The measured gains were obtained through gain comparison method. The simulated and measured peak gains of the 8×8 array are

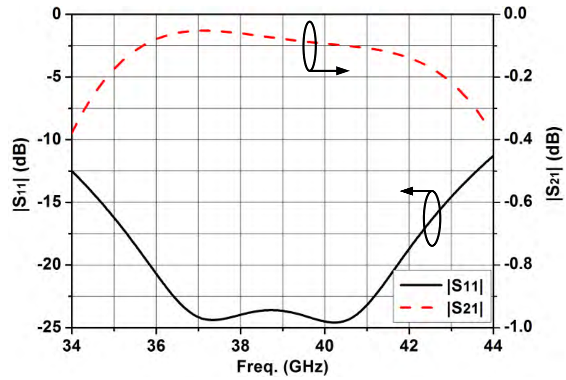


**FIGURE 16.** Simulated S-parameters of waveguide to SIW transition.

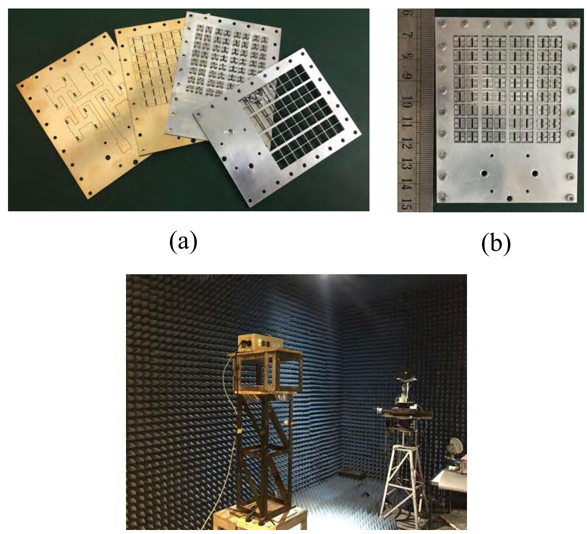

(a) (b)

(c)

**FIGURE 17.** (a) Photo of the disassembled fabricated 8×8 antenna array. (b) Photo of the assembled antenna. (c) Measurement setup.

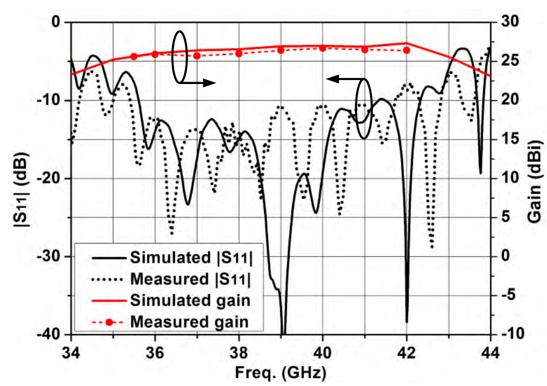


**FIGURE 18.** Simulated and measured $|S_{11}|$ and gains of the proposed 8×8 array antenna.

27.3 dBi at 42 GHz and 26.7 dBi at 40 GHz, respectively. The simulated radiation efficiencies of the antenna array are above 90% within the impedance bandwidth. The measured radiation efficiency can be calculated by comparing

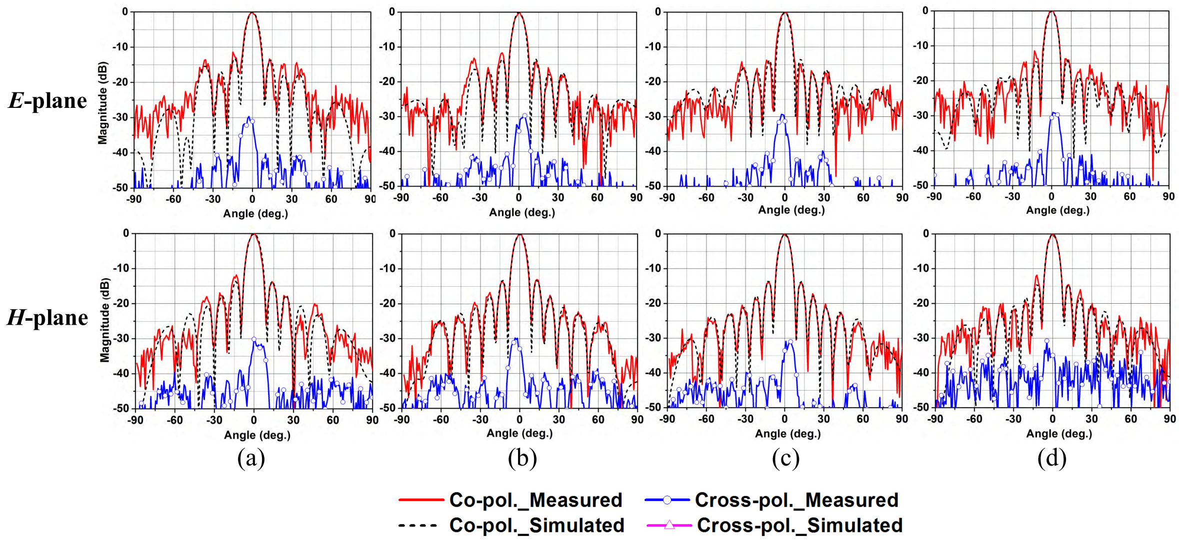


**FIGURE 19.** **Simulated and measured radiation patterns for the proposed 8×8 antenna array. (a) 36 GHz. (b) 38 GHz. (c) 40 GHz. (d) 42 GHz.**

the simulated directivity and the measured gain [33]. Then the measured radiation efficiency of the 8×8 array is 83.2% at 40 GHz. The aperture area of the 8×8 antenna array is defined as 49.5 mm×49.1 mm. The aperture efficiency, $\eta$, can be calculated by the following equation [35]:

$$\eta = \frac{G\lambda^2}{4\pi S} \tag{1}$$

where $G$ and $S$ are the measured gain and the physical aperture of the antenna, respectively. Then, the aperture efficiency of the antenna array can be calculated as 86.1% at 40 GHz. The comparisons of simulated and measured radiation patterns in the $E(xoz)$- and $H(yoz)$-planes for the 8×8 antenna array are shown in Fig. 19 for frequencies at 36, 38, 40 and 42 GHz. Broadside and stable radiation patterns are observed. The measured first sidelobe levels of radiation patterns are lower than −11 dB across the bandwidth. The slight discrepancy between the measured and simulated first sidelobe levels is mainly resulted from fabrication tolerance and the influence of the feeding setup near the antenna in measurement. The measured cross-polarization levels are lower than −29 dB within the bandwidth in both planes. With the contributions from the high-gain antenna elements and low-loss SIW feeding network, good radiation performance is achieved.

In this design, the two PCB substrates and aluminum plates are fixed by screws and the effects of possible air gaps between them should be considered [18]. To simplify the analysis, the thicknesses of the gap between two PCBs and the gap between PCB and aluminum plates are set to be the same. The simulated results of the 8×8 antenna array with different thicknesses of the air gaps are presented in Fig. 20. It can be seen that the effect of the air gaps can be ignored when the thickness is less than 0.02 mm. When the thickness of the air gaps reach 0.05 mm and 0.1 mm, the impedance matching deteriorates which results in that $|S_{11}|$ is greater than −10 dB at some frequencies and the gain decreases within the bandwidth. It can be concluded that the possible air gaps would degrade the performance of the fabricated antenna

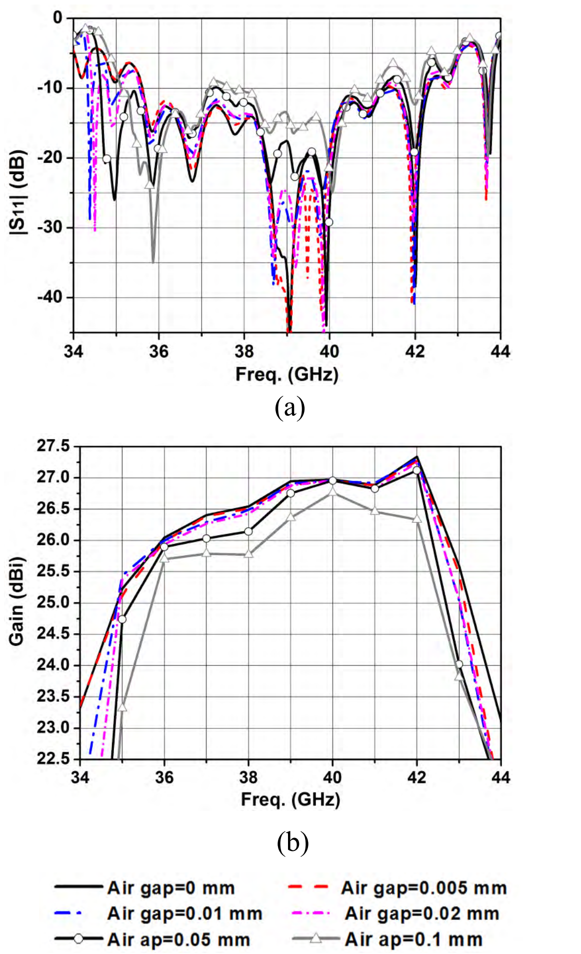


**FIGURE 20.** **Simulated results of the 8×8 array with different thicknesses of the air gaps. (a) $|S_{11}|$. (b) Gains.**

**TABLE 5.** Comparison Between Proposed And Reported Millimeter-Wave Antenna Arrays.

| Ref. | Type | Total Size ($\lambda_0$) | No. of Elements | BW | Gain (dBi) | Max. Radiation Efficiency |
|---|---|---|---|---|---|---|
| [19] | SIW-fed spiral array (PCB) | n.a. | 4×4 | 14.1% (56.55-65.13 GHz) | 19.5 dBic | 87.1% |
| [20] | SIW-fed cavity-backed patch array (PCB) | 6.33 × 7.08 × 0.854 | 8×8 | 14.1% (58.2-67 GHz) | 26 | 68.5% |
| [23] | SIW-fed cavity array (LTCC) | 9.4×6.2 | 8×8 | 17.1% (54.86-65.12 GHz) | 22.1 | 54.7% |
| [25] | Dielectric-loaded SIW slot array (LTCC) | 12.79×8.68×0.502 | 8×8 | 15.3% (126.8-147.8 GHz) | 21.3 | 35% |
| [27] | SIW-fed cavity array (LTCC) | 6.72×6.72×0.48 | 8×8 | 14.9% (87-101 GHz) | 22.9 | n.a. |
| [30] | SIW-fed ME-dipole array (PCB) | 6.22×6.91 | 8×8 | 18.2% (55.4-66.5 GHz) | 26.1 dBic | 75% |
| [31] | ME-dipole array fed by printed ridge gap waveguide (PCB) | 3.5×3.4×0.28 | 4×4 | 16.5% (28.8-34 GHz) | 21.2 | 70%* |
| [32] | ME-dipole array fed by metallic gap waveguide (PCB) | 8.32×5.44×3.68 | 1×8 | 14.1% (89-102.5 GHz) | 18 | n.a. |
| [33] | SIW-fed ME-dipole array (PCB) | n.a. | 8×8 | 22.9% (56.1-70.6 GHz) | 26.7 | 80%** |
| **This Work** | **SIW-fed ME dipole array (PCB)** | **8.47×10.96×0.847** | **8×8** | **16.3% (35.4-41.7 GHz)** | **26.7** | **83.2% (90%**)** |

* Measured total efficiency.
** Simulated radiation efficiency.

array. However, the possible air gap between different PCB layers can be avoided by adding the bonding film or glue in practical applications [18].

Performances of different kinds of MMW antenna arrays are listed in Table 5 for a comparison with our work. In [30]-[33], four kinds of printed ME-dipole arrays fed by SIW or gap waveguide are designed on PCB substrates. Excellent performances such as broad bandwidth and high gain of the arrays have been achieved. However, the dielectric loss caused by the substrates under the radiating structures decreases the radiation efficiency of the arrays. In the proposed design, each radiating ME-dipole element composes of metallic posts and cavity wall which avoid substrate loss and lead to a high radiation efficiency. It is observed that the proposed design has advantages such as broad bandwidth, high gain, and high radiation efficiency. It is noted that many of the reported multilayered SIW-fed MMW antenna arrays were fabricated in LTCC process which leads to relatively high cost. The proposed design provides an approach for broadband, high-gain and low-cost MMW antenna array design in PCB process.

## V. CONCLUSION

A broadband and high-gain SIW-fed antenna array has been presented for 5G applications. The wideband and high-gain antenna element is composed of two dipoles and a cavity which enhances the antenna performance. Combined with the low-loss two-layer SIW feeding network, an 8×8 prototype with an impedance bandwidth of 16.3% and a gain up to 26.7 dBi has been designed and measured to verify the design method. Stable radiation performances have been achieved. It demonstrates that the proposed antenna array is suitable for 5G communication applications.

## REFERENCES

[1] Federal Communications Commission. (2016). *Fact Sheet: Spectrum Frontiers Rules Identify, Open Up VAST Amounts of New High-Band Spectrum for Next Generation (5G) Wireless Broadband*. [Online]. Available: https://apps.fcc.gov/edocs_public/attachmatch/DOC-340310A1.pdf

[2] W. Yang, K. Ma, K. S. Yeo, and W. M. Lim, "A compact high-performance patch antenna array for 60-GHz applications," *IEEE Antennas Wireless Propag. Lett.*, vol. 15, pp. 313–316, 2016.

[3] T. Sehm, A. Lehto, and A. V. Raisanen, "A high-gain 58-GHz box-horn array antenna with suppressed grating lobes," *IEEE Trans. Antennas Propag.*, vol. 47, no. 7, pp. 1125–1130, Jul. 1999.

[4] G. Montisci, G. Mazzarella, and G. A. Casula, "Effective Analysis of a Waveguide Longitudinal Slot With Cavity," *IEEE Trans. Antennas Propag.*, vol. 60, no. 7, pp. 3104–3110, Jul. 2012.

[5] Y. Miura, J. Hirokawa, M. Ando, Y. Shibuya, and G. Yoshida, "Double-layer full-corporate-feed hollow-waveguide slot array antenna in the 60-GHz band," *IEEE Trans. Antennas Propag.*, vol. 59, no. 8, pp. 2844–2851, Aug. 2011.

[6] D. Deslandes and K. Wu, "Integrated microstrip and rectangular waveguide in planar form," *IEEE Microw. Wireless Compon. Lett.*, vol. 11, no. 2, pp. 68–70, Feb. 2001.

[7] H. Uchimura, T. Takenoshita, and M. Fujii, "Development of a 'laminated waveguide,'" *IEEE Trans. Microw. Theory Techn.*, vol. 46, no. 12, pp. 2438–2443, Dec. 1998.

[8] N. Ghassemi, K. Wu, S. Claude, X. Zhang, and J. Bornemann, "Low-cost and high-efficient W-band substrate integrated waveguide antenna array made of printed circuit board process," *IEEE Trans. Antennas Propag.*, vol. 60, no. 3, pp. 1648–1653, Mar. 2012.

[9] N. Ghassemi and K. Wu, "High-efficient patch antenna array for E-band gigabyte point-to-point wireless services," *IEEE Antennas Wireless Propag. Lett.*, vol. 11, pp. 1261–1264, 2012.

[10] O. Kramer, T. Djerafi, and K. Wu, "Very small footprint 60 GHz stacked Yagi antenna array," *IEEE Trans. Antennas Propag.*, vol. 59, no. 9, pp. 3204–3210, Sep. 2011.

[11] T. Y. Yang, W. Hong, and Y. Zhang, "Wideband millimeter-wave substrate integrated waveguide cavity-backed rectangular patch antenna," *IEEE Antennas Wireless Propag. Lett.*, vol. 13, pp. 205–208, 2014.

[12] L. Wang, Y. J. Cheng, D. Ma, and C. X. Weng, "Wideband and dual-band high-gain substrate integrated antenna array for E-band multi-gigahertz capacity wireless communication systems," *IEEE Trans. Antennas Propag.*, vol. 62, no. 9, pp. 4602–4611, Sep. 2014.

[13] Y. J. Cheng, Y. X. Guo, and Z. G. Lin, "W-band large-scale high-gain planar integrated antenna array," *IEEE Trans. Antennas Propag.*, vol. 62, no. 6, pp. 3370–3373, Jun. 2014.

[14] J. Wu, Y. J. Cheng, and Y. Fan, "A wideband high-gain high-efficiency hybrid integrated plate array antenna for V-band inter-satellite links," *IEEE Trans. Antennas Propag.*, vol. 63, no. 4, pp. 1225–1233, Apr. 2015.

[15] B. Liu *et al.*, "Substrate integrated waveguide (SIW) monopulse slot antenna array," *IEEE Trans. Antennas Propag.*, vol. 57, no. 1, pp. 275–279, Jan. 2009.

[16] Y. Li and K.-M. Luk, "Wideband perforated dense dielectric patch antenna array for millimeter-wave applications," *IEEE Trans. Antennas Propag.*, vol. 63, no. 8, pp. 3780–3786, Aug. 2015.

[17] Y. J. Cheng, W. Hong, and K. Wu, "94 GHz substrate integrated monopulse antenna array," *IEEE Trans. Antennas Propag.*, vol. 60, no. 1, pp. 121–129, Jan. 2012.

[18] Y. Li and K.-M. Luk, "Low-cost high-gain and broadband substrate-integrated-waveguide-fed patch antenna array for 60-GHz band," *IEEE Trans. Antennas Propag.*, vol. 62, no. 11, pp. 5531–5538, Nov. 2014.

[19] Q. Zhu, K.-B. Ng, and C. H. Chan, "Printed circularly polarized spiral antenna array for millimeter-wave applications," *IEEE Trans. Antennas Propag.*, vol. 65, no. 2, pp. 636–643, Feb. 2017.

[20] J. Wu, Y. J. Cheng, and Y. Fan, "60-GHz substrate integrated waveguide fed cavity-backed aperture-coupled microstrip patch antenna arrays," *IEEE Trans. Antennas Propag.*, vol. 63, no. 3, pp. 1075–1085, Mar. 2015.

[21] H. Jin, W. Che, K.-S. Chin, W. Yang, and Q. Xue, "Millimeter-wave $TE_{2}0$-mode SIW dual-slot-fed patch antenna array with a compact differential feeding network," *IEEE Trans. Antennas Propag.*, vol. 66, no. 1, pp. 456–461, Jan. 2018.

[22] Y. Li and K.-M. Luk, "60-GHz dual-polarized two-dimensional switch-beam wideband antenna array of aperture-coupled magneto-electric dipoles," *IEEE Trans. Antennas Propag.*, vol. 64, no. 2, pp. 554–563, Feb. 2016.

[23] J. F. Xu, Z. N. Chen, X. M. Qing, and W. Hong, "Bandwidth enhancement for a 60 GHz substrate integrated waveguide fed cavity array antenna on LTCC," *IEEE Trans. Antennas Progag.*, vol. 59, no. 3, pp. 826–832, Mar. 2011.

[24] W. C. Yang, H. Wang, W. Q. Che, Y. Huang, and J. Wang, "High-gain and low-loss millimeter-wave LTCC antenna array using artificial magnetic conductor structure," *IEEE Trans. Antennas Propag.*, vol. 63, no. 1, pp. 390–395, Jan. 2015.

[25] J. Xu, Z. N. Chen, X. Qing, and W. Hong, "140-GHz $TE_{20}$-mode dielectric-loaded SIW slot antenna array in LTCC," *IEEE Trans. Antennas Propag.*, vol. 61, no. 4, pp. 1784–1793, Apr. 2013.

[26] H. Jin, W. Che, K.-S. Chin, G. Shen, W. Yang, and Q. Xue, "60-GHz LTCC differential-fed patch antenna array with high gain by using soft-surface structures," *IEEE Trans. Antennas Propag.*, vol. 65, no. 1, pp. 206–216, Jan. 2017.

[27] B. Cao, H. Wang, Y. Huang, and J. Zheng, "High-gain L-probe excited substrate integrated cavity antenna array with LTCC-based gap waveguide feeding network for W-band application," *IEEE Trans. Antennas Propag.*, vol. 63, no. 12, pp. 5465–5474, Dec. 2015.

[28] J. Xu, Z. N. Chen, X. Qing, and W. Hong, "140-GHz planar broadband LTCC SIW slot antenna array," *IEEE Trans. Antennas Propag.*, vol. 60, no. 6, pp. 3025–3028, Jun. 2012.

[29] K.-M. Luk and H. Wong, "A new wideband unidirectional antenna element," *Int. J. Microw. Opt. Technol.*, vol. 1, no. 1, pp. 35–44, Jun. 2006.

[30] Y. Li and K.-M. Luk, "A 60-GHz wideband circularly polarized aperture-coupled magneto-electric dipole antenna array," *IEEE Trans. Antennas Propag.*, vol. 64, no. 4, pp. 1325–1333, Apr. 2016.

[31] M. S. Sorkherizi, A. Dadgarpour, and A. A. Kishk, "Planar high-efficiency antenna array using new printed ridge gap waveguide technology," *IEEE Trans. Antennas Propag.*, vol. 65, no. 7, pp. 3772–3776, Jul. 2017.

[32] J. Cao, H. Wang, S. Mou, S. Quan, and Z. Ye, "W-band high-gain circularly polarized aperture-coupled magneto-electric dipole antenna array with gap waveguide feed network," *IEEE Antennas Wireless Propag. Lett.*, vol. 16, pp. 2155–2158, 2017.

[33] Q. Zhu, K. B. Ng, C. H. Chan, and K.-M. Luk, "Substrate-integrated-waveguide-fed array antenna covering 57–71 GHz band for 5G applications," *IEEE Trans. Antennas Propag.*, vol. 65, no. 12, pp. 6298–6306, Dec. 2017.

[34] K. M. Luk *et al.*, "A microfabricated low-profile wideband antenna array for terahertz communications," *Sci. Rep.*, vol. 7, no. 1, p. 1268, 2017.

[35] J. Volakis, *Antenna Engineering Handbook*, 4th ed. New York, NY, USA: McGraw-Hill, 2009, pp. 1–7.

**XIUPING LI** (M'05–SM'07) received the B.S. degree from Shandong University in 1996, and the Ph.D. degree from the Beijing Institute of Technology in 2001. From 2001 to 2003, she was a Research Fellow with the Nanyang Technological University of Singapore. In 2003, she was a Research Professor at Yonsei University, Seoul, South Korea. Since 2004, she joined the Beijing University of Posts and Telecommunications as an Associate Professor, and was promoted to the post of Professor in 2009.

She has authored four books, and over 100 journal and conference papers. Her current research interests include millimeter-wave and THz antennas, RFID systems, and RF MMIC design. She has been selected into the New Century Excellent Talents Support Plan in the National Ministry of Education, Beijing Science & Technology Nova Support Plan, in 2007 and 2008, respectively. She received the Second Prize of Progress in Science and Technology, Chinese Institute of Communications, in 2015. She was a recipient of the awards of the Distinguished Youth Teacher of Beijing in 2017, and the Excellent Teacher of Beijing in 2017. She has also been a recipient of over 20 PRC patents.

**JUN XIAO** received the B.Eng. and M.Eng. degrees from the Harbin Institute of Technology, Harbin, China, in 2008 and 2011, respectively. He is currently pursuing the Ph.D. degree in electronic science and technology with the Beijing University of Posts and Telecommunications, Beijing, China. His research interests include UWB antennas, millimeter-wave antennas, and THz antennas.

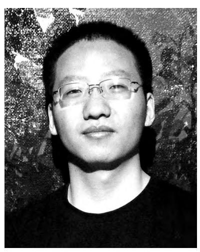

**ZIHANG QI** (S'17) received the B.Eng. degree in 2013. He is currently pursuing the Ph.D. degree with the Beijing University of Posts and Telecommunications. His current research interests include millimeter-wave/THz antennas and microwave filters.

**HUA ZHU** (M'17) received the M.S. degree from the Guilin University of Electronic Technology, Guilin, China, in 2010, and the Ph.D. degree from the Beijing University of Posts and Telecommunications, Beijing, China, in 2015. She is currently a Lecturer with the Beijing University of Posts and Telecommunications, Beijing. Her research interests include UHF RFID beam scanning antenna array design in complex environment and millimeter wave/Terahertz antenna design.